ACS Sustainable Chemistry & Engineering

Research Article

pubs.acs.org/journal/ascecg

Sustainable Preparation of Copper Particles Decorated Carbon Microspheres and Studies on Their Bactericidal Activity and Catalytic Properties

Xinxin Cheng,[†] Aiping Fu,[†] Hongliang Li,[*,†] Yiqian Wang,[‡] Peizhi Guo,[†] Jingquan Liu,[†] Jintao Zhang,[†] and Xiu Song Zhao[†,§]

[†]Collaborative Innovation Center for Marine Biomass Fibers, Laboratory of New Fiber Materials and Modern Textile, Growing Base for State Key Laboratory, College of Chemical Science and Engineering, Qingdao University, No. 308 Ningxia Road, Qingdao 266071, China

[‡]College of Physics, Qingdao University, No. 308 Ningxia Road, Qingdao 266071, China

[§]School of Chemical Engineering, The University of Queensland, St Lucia, Brisbane, QLD 4072, Australia

Supporting Information

ABSTRACT: Cu particles decorated carbon composite microspheres (CCMs) with a unique sesame ball structure have been prepared by combining the mass-producible spray drying technique with calcinations. The conventional cuprammonium cellulose complex solution obtained by dissolving cellulose in a cuprammonia solution has been applied as raw materials for the preparation of $Cu(NH_3)_4^{2+}$/cellulose complex microspheres via a spray drying process. The resulted $Cu(NH_3)_4^{2+}$/cellulose complex microspheres are then transformed into the Cu particles homogeneously decorated porous carbon spheres *in situ* by calcinations at 450 or 550 °C. The coordination effect between the $Cu(NH_3)_4^{2+}$ species and the hydroxyl groups of the cellulose macromolecules has been exploited for directing the dispersion of the Cu particles in the resultant composite CCMs. The antimicrobial effects of the CCMs are evaluated by determining the minimum growth inhibitory concentrations using *Staphylococcus aureus* and *Escherichia coli* as representatives, respectively. The CCMs show high efficiency catalytic properties to the conversion of 4-nitrophenol to 4-aminophenol using $NaBH_4$ as a reductant in a mild condition. The recyclability and stability of the CCM catalysts have also been studied.

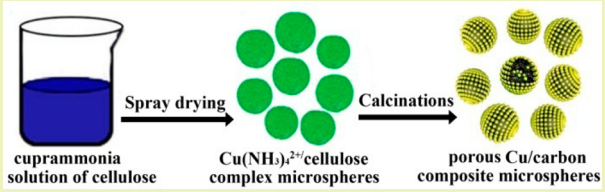

KEYWORDS: *Copper particles, Cuprammonium cellulose complex, Chelating effect, Porous carbon microspheres, Antibacterial activity, Supported catalyst*

INTRODUCTION

Copper (Cu) is an inexpensive metal that exhibits electronic, catalytic, optical, and antifungal/antibacterial properties similar to those of noble metals.[1,2] Cu nanoparticles are considered as a viable alternative to noble metal nanoparticles in certain fields such as antibacterial application, organic synthesis, and electrocatalytic reaction,[3,4] and they were intensively investigated during the past decade.[5−7] However, Cu nanoparticles are known to be extremely sensitive to oxygen by forming copper oxide nanoparticles and are also apt to aggregate into large sized aggregation due to their high surface energy and high reactivity, resulting in the deterioration of their unique properties.[8,9] So, it is desirable to use a matrix that could bind the Cu particles and protect them from oxidizing environment.[10] Consequently, dispersion of Cu nanoparticles on a substrate especially a porous one is favorable: (1) they can be easily isolated by precipitation, ultracentrifugation, or ultrafiltration and then recycled; (2) the high dispersion of catalyst nanoparticles on the surface of porous substrate allows the reactant molecules to easily access to the active site of the catalyst, therefore accelerating the chemical conversion.[11,12] Porous carbon material has been regarded as one of the most promising substrates for supporting metallic nanoparticles due to their high specific surface area, fine chemical durability, and high biocompatibility.[13,14] However, it is worth mentioning that dispersions of nanoparticles are intrinsically and thermodynamically metastable.[15] Uniform dispersion of the nanoparticles is dictated by the activation energy, especially on the surface of a porous substrate. When the activation energy is insufficient to affect dispersion, an agglomeration of the small sized particles or an increase of individual particle size has been observed.[16] Thus, highly dispersed nanoparticles are only kinetically stabilized and cannot be prepared under conditions that exceed a threshold.[17] Hence, the development of a cost-effective method for utilizing Cu particles would prove to be quite beneficial. As a requirement, the use of surface-stabilizing

Received: May 2, 2015
Revised: September 7, 2015
Published: September 11, 2015

DOI: 10.1021/acssuschemeng.5b00382
ACS Sustainable Chem. Eng. 2015, 3, 2414−2422

agents has been exploited in synthesizing Cu nanomaterials to hinder sintering, recrystallization, and aggregation. On the other hand, the supply of porous carbon substrates with spherical morphology is still problematic because there is a lack of efficient and environmentally friendly method to prepare porous carbon microspheres in large, especially that utilizing low cost raw materials.[18]

As the most abundant renewable natural polymer on earth, cellulose is a promising raw material in chemical, biological, and energy industries.[19] It can be used as a kind of low-cost precursor to prepare porous carbon materials.[20] Utilization of cellulose is certainly beneficial for the environment and sustainable development because it is a biocompatible, biodegradable, and renewable resource. However, the preparation of porous carbon spheres with cellulose as the carbon source encounters difficulties due to the low solubility of cellulose in normal aqueous solvent. As one of the oldest solvent for cellulose, cuprammonia has been utilized to dissolve cellulose macromolecules in the spinning industry for more than 100 years.[21] While, the utilization of the resultant cellulose cuprammonia solution was devoted mainly to the preparations of cuprammonuium for the textile industry or cellulose based hemodialysis membrane for medical application.

In this paper, we reported on a facile and mass-producible approach to the preparation of Cu particles *in situ* decorated carbon microspheres. The mass-producible technique and industrial preparation method for powders, namely spray drying, was conveyed to the preparation of $Cu(NH_3)_4^{2+}$/cellulose complex microspheres using the traditional cellulose cuprammonia aqueous solution as a raw material. The conventional cuprammonia cellulose aqueous solution, which is composed of $Cu(NH_3)_4^{2+}$/cellulose complexes, was obtained by dissolving cellulose with cuprammonia aqueous solution. By calcining the resulted $Cu(NH_3)_4^{2+}$/cellulose complex microspheres at 450 or 550 °C, the cellulose macromolecules were carbonized, whereas the $Cu(NH_3)_4^{2+}$ moieties decomposed and were reduced by cellulose, forming Cu particles homogeneously decorated carbon microspheres *in situ* (abbreviated to Cu/carbon microspheres and denoted by CCMs). For the total preparation, the $Cu(NH_3)_4^{2+}$ species played two different roles, i.e., as a solving agent in the preparation of cuprammonia cellulose solution and as a precursor for the Cu particles of CCMs. The chelating effect between the hydroxyl groups of the cellulose macromolecules and the $Cu(NH_3)_4^{2+}$ species has been exploited for controlling the dispersion of the Cu particle in the resultant composite CCMs. Interestingly, the resultant CCMs can be hollow with the increase of the content of cellulose in the cellulose cuprammonia aqueous solution. The CCMs possess a unique structure like the sesame balls and as a result, remarkable antibacterial and catalytic properties were bestowed on this novel structure. The antimicrobial effect was quantified based on the inhibition rate tests, and also by determining the minimum inhibitory concentrations (MIC) using Gram-positive *Staphylococcus aureus* and Gram-negative *Escherichia coli* as representatives, respectively.[22,23] The resultant CCMs also showed highly activity in catalytic conversion of 4-nitrophenol (4-NP) to 4-aminophenol (4-AP) using $NaBH_4$ as a reductant performed in an aqueous solution under mild conditions and furthermore they can be used as Fenton-catalyst for the degradation of other kind of organics with H_2O_2, such as methyl orange.

EXPERIMENTAL SECTION

Materials. Cellulose with a viscosity-average molecular weight of 8.5×10^4 was obtained from Hailong Chemical Fiber Co., Ltd. Sodium hydroxide, copper sulfate, ammonium hydroxide, sodium borohydride ($NaBH_4$), and 4-nitrophenol were analytical grade and used as received without further purification. Distilled water was used in all the experiments.

Preparation of Cuprammonia Solution of Cellulose. 25 mL of 10 wt % NaOH aqueous solution was added into 100 mL of 5 wt % copper sulfate aqueous solution dropwise until the Cu^{2+} was precipitated completely. After that, the blue sediment was separated by centrifugation and washed thrice with distilled water. The precipitate was then dissolved completely by concentrated aqueous ammonia under stirring. The freshly obtained cuprammonia was utilized for the rapid dissolution of cellulose for 30 min, obtaining blue cuprammonia aqueous solution of cellulose. The concentration of the cellulose was controlled by dissolving different amounts of cellulose with a fixed quantity of cuprammonia. The concentration of the resultant cuprammonia cellulose solution is described using the mass ratio of copper sulfate over cellulose, for example 5:0.5, 5:1.0, 5:1.5, and 5:2, in which 5 means the grams of copper sulfate used for preparing cuprammonia, whereas 0.5, 1.0, etc. stand the amounts of dissolved cellulose.

Preparation of $Cu(NH_3)_4^{2+}$/Cellulose Complex Microspheres. The $Cu(NH_3)_4^{2+}$/cellulose complex microspheres were prepared by a spray drying process using the cuprammonia aqueous solution of cellulose as starting materials through a laboratory-scale SP-1500 spray dryer (Shanghai SunYi Tech Co., Ltd.). The cellulose cuprammonia aqueous solution was sprayed into the chamber of the spray dryer at 160 °C using hot air as carrier gas. Dried $Cu(NH_3)_4^{2+}$/cellulose complex microspheres were collected by a connected cyclone separator. The inlet cellulose cuprammonia aqueous solution was pulverized by the shear forces of the pressurized air with a pressure in the range of 200−400 kPa, spraying out tiny droplets of cellulose cuprammonia solution through the orifice of the nozzle on the spray dryer. The moisture in these droplets are quickly evaporated upon contacting with the hot air flow through the chamber, resulting in drying-out and stable porous $Cu(NH_3)_4^{2+}$/cellulose complex microspheres.

Preparation of CCMs. The CCMs were facilely prepared by calcining the $Cu(NH_3)_4^{2+}$/cellulose complex microspheres in a N_2 atmosphere. The calcinations were performed in a programmed tubular furnace at 450 or 550 °C for 3 h, respectively. The resulted CCMs were named as CCM-450(x:y) and CCM-550(x:y) (x:y = 5:0.5, 5:1.0, 5:1.5, and 5:2), respectively, where 450 and 550 represent the calcination temperature, whereas the ratio in the brackets refers to the applied cuprammonia solution of cellulose as described above.

Antibacterial Properties. The antibacterial activities of the CCM samples against *E. coli* (ATCC25922) and *S. aureus* (ATCC6538) were performed by broth dilution method and the plate counting method with reference to Nation Standard of China GB/T 20944 (for more details on the test procedures, please refer to the Supporting Information).[24]

Catalytic Reduction of 4-NP. The catalytic reduction of 4-NP was carried out in a standard quartz cuvette and the process was monitored by a UV−vis spectrophotometer to examine the catalytic activity of the CCMs in the presence of an excess amount of $NaBH_4$ at room temperature. A typical procedure was as follows: 2.0 mL of ultrapure water, 0.1 mL of 4-NP solution (0.005 mol/L), and 1.0 mL of freshly prepared $NaBH_4$ aqueous solution (0.2 mol/L) were added into a quartz cuvette. Then the color of solution turned to bright yellow immediately. At this stage, the nitrophenol converted to nitrophenolate anion. Subsequently, 5 mg of CCMs was added to the solution, then monitored by measuring the adsorption at λ_{max} = 400 nm every 1.5 min using a UV−vis spectrophotometer. As the reaction proceeded, the peak at λ_{max} = 400 nm corresponding to the *p*-nitrophenolate ion disappeared due to its conversion to *p*-aminophenolate ions with time goes and the solution changed gradually from bright yellow to transparent.[25] The influences of Cu content in CCMs

DOI: 10.1021/acssuschemeng.5b00382
ACS Sustainable Chem. Eng. 2015, 3, 2414−2422

on the catalytic properties, the effects of dose of the applied composite catalysts, the concentration of 4-NP and $NaBH_4$, and the recyclability of the catalyst were also investigated. As control experiment, a similar reaction was performed using porous carbon particles as the catalyst (Cu was removed by acid etching) instead of CCMs.

Recyclability and Stability Test. To test the recyclability of the catalyst, five successive cycles of catalytic reduction were carried out employing a definite amount of catalyst. In the successive cycles, the catalyst was collected by centrifugation from the solution and washed with ethanol and water several times, and used for the next cycling. The stability of Cu particles in the CCMs upon storing in ambient air for 6 months and after 5 cycles of the catalytic reaction has been investigated by monitoring their XRD patterns.

Characterizations. The morphologies and structures of the samples were analyzed using a JEOL JSM-7500F scanning electron microscopy (SEM) instrument and a JEOL JEM-2100F transmission electron microscopy (TEM) instrument. Elemental mapping analyses were performed using an energy disperse spectroscopy (EDS) attached to the SEM equipment. Thermogravimetric analysis (TGA) was performed using a SDT 2960 DSC-TGA, TA Instruments (Wilmington, USA), at a ramp of 5 °C/min between 0 and 700 °C in nitrogen. The specific surface areas were estimated using the Brunauer–Emmett–Teller (BET) method with a TriStar 3000 surface area and pore analyzer (Micromeritics). Powder X-ray diffraction (XRD) patterns were collected using a Bruker D8 Advance X-ray diffractometer equipped with graphite monochromatized Cu Kα radiation (λ = 0.154 18 nm). A TAS-986 flame atomic absorption spectrophotometry (FAAS) instrument was used for the detection of the copper contents in the composite spheres by dissolving the Cu particles with dilute aqueous solution of nitric acid. UV–vis spectra were measured through a TU-1901 UV–visible spectrophotometer (Purkinje General). The X-ray photoelectron spectra were accumulated on a Thermo Scientific ESCALAB 250 multitechnique electron spectrometer system with an Al KR standard X-ray source, and the binding energies were calibrated by C 1s.

RESULTS AND DISCUSSION

XRD Measurements. Figure 1 depicts the XRD patterns of CCM-450 series samples prepared with the cuprammonia

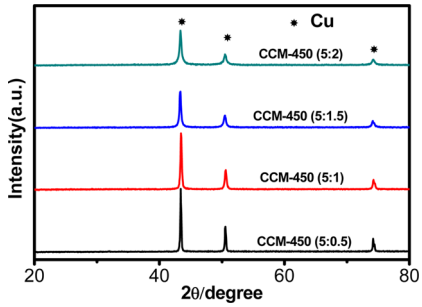

Figure 1. XRD patterns of the CCM-450 series samples.

cellulose solution made of $CuSO_4$/cellulose with mass ratios of 5:0.5, 5:1, 5:1.5, and 5:2, respectively. Three characteristic peaks were observed at 2θ values of 43.3°, 50.4°, and 74.1°, which respectively correspond to the (111), (200), and (220) crystalline planes of a face-centered cubic (fcc) copper phase (PDF No. 04-0836). No diffraction peak of CuO, Cu_2O, or other copper oxide is observed in the patterns, indicating that all the $Cu(NH_3)^{2+}$ complexes have been reduced to metallic Cu.[26] The sharp and strong peaks also reveal that Cu particles in the CCMs are highly crystallized. Similar XRD patterns were obtained for the CCM-550 samples (see Figure S1). Whereas, no diffraction peaks were observed for the $Cu(NH_3)_4^{2+}$/cellulose complexes due to their amorphous nature. The formation of metallic Cu can be ascribed to the reductive atmosphere created due to the thermal decomposition of cellulose. The $Cu(NH_3)_4^{2+}$ species were reduced to metallic Cu during the calcinations of these $Cu(NH_3)_4^{2+}$/cellulose complex spheres. The mass contents of Cu detected by FAAS are about 92, 87, 78, and 72 wt % for CCM-450(x:y) series samples (where x:y = 5:0.5, 5:1, 5:1.5, and 5:2, respectively). Carbon contents of about 8, 13, 22, and 28 wt % in the corresponding CCMs can then be deduced by deducting the Cu content from the composite spheres. Similar values were obtained for CCM-550(x:y) series samples.

SEM and TEM Measurements. SEM images of the spray dried $Cu(NH_3)_4^{2+}$/cellulose complex microspheres are depicted in Figure S2. The microspheres showed a smooth surface and a relative broad size distribution from 1 to 5 μm. In comparison with images A, B, and C, image D contains some broken microspheres. This can be explained as the formation of hollow structured $Cu(NH_3)_4^{2+}$/cellulose microspheres due to the high viscosity of the copper ammonia cellulose solution with large cellulose content. A phenomenon that the fluffiness of the powders turned to more obvious along with the increase of cellulose content in the copper ammonia cellulose solution, which can support the above speculation, has been observed for the collected $Cu(NH_3)_4^{2+}$/cellulose microspheres. Figure 2 shows the images of CCMs derived from the corresponding $Cu(NH_3)_4^{2+}$/cellulose complex microspheres as presented in Figure S2 by calcinations under nitrogen for 3 h at different temperatures. It can be readily discerned from Figure 2 that for both CCM-450 series and CCM-550 series samples, the Cu particles appeared on the surfaces of the composite spheres turned to more uniform and well-dispersed with the increase of cellulose content in the complex microspheres. In comparison with that in CCM-450 series samples, the copper particles in CCM-550 series samples made from the same cellulose content are little bit larger (see images A and E, B and F, C and G, D and H), and it can also be seen that the morphology of the CCM-550 series samples turned to irregular, especially for that derived from complex microspheres with a low cellulose content (i.e., image E). The difference between the two series samples can be ascribed to the different calcination temperatures. During the calciantion process of the $Cu(NH_3)_4^{2+}$/cellulose complex spheres, cellulose was carbonized and formed the spherical carbon matrices, while $Cu(NH_3)_4^{2+}$ decomposed in concurrence and reduced to metallic Cu nanoparticles. Meanwhile, the resultant Cu nanoparticles diffused from the inner of the carbon matrixes to the surface, forming the CCM spheres with a novel sesame ball structure. The coordination effect between the $Cu(NH_3)_4^{2+}$ species and the hydroxyl groups of the cellulose macromolecules plays important role in directing the dispersion of the Cu particle in the composite CCMs. With the increase of calcination temperature from 450 to 550 °C, small sized Cu nanoparticles melted and fused into large sized ones. As a result, significant coarsening occurs as the grain grows at the expense of the small Cu particles (see Figure 2A). Interestingly, several broken spheres in images of D and H reveal that the spheres are hollow-structured. A more detailed structure investigation of these CCM samples were performed further by TEM measurement and the results will be discussed in the following sections.

The TEM images of two series of CCMs obtained at temperatures of 450 and 550 °C, respectively, were depicted in Figure S3. It can be seen that Cu particles successfully grew on the surface of the carbon substrate, and a small quantity of Cu

DOI: 10.1021/acssuschemeng.5b00382
ACS Sustainable Chem. Eng. 2015, 3, 2414–2422

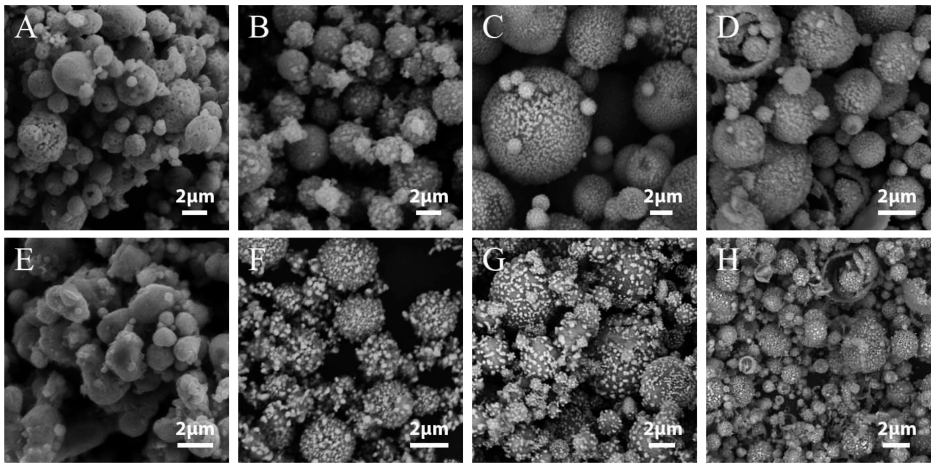

Figure 2. SEM images of CCMs derived from the corresponding $Cu(NH_3)_4^{2+}$/cellulose microspheres as presented in Figure S2 by calcinations in nitrogen for 3 h at different temperatures. (A) CCM-450(5:0.5), (B) CCM-450(5:1), (C) CCM-450(5:1.5), and (D) CCM-450(5:2); (E) CCM-550(5:0.5), (F) CCM-550(5:1), (G) CCM-550(5:1.5), and (H) CCM-550(5:2).

particles still embedded in the matrix of carbon spheres. For both the two series CCMs, with the increase of cellulose content, the CCM spheres transformed from solid ones (see images A, B, E, and F) to hollow ones (see images C, D, G, and H); meanwhile, the Cu particles in the CCMs turned to small sized ones and their distribution became more homogeneous. The transformation of CCMs from solid spheres to hollow ones might be due to the changing of the viscosity of the cuprammonia aqueous solution of cellulose with the increase of cellulose content. In comparison of pictures of CCM-450 series samples (images A to D) with those of CCM-550 series samples (images E to H), one can find out that the sizes of Cu particles in the CCM-450 series samples are slightly smaller than those in the CCM-550 ones derived from $Cu(NH_3)_4^{2+}$/cellulose complex spheres with the same cellulose content but calcined at different temperatures. This may be due to the sintering effect of nanosized copper particles at a relative high calcination temperature. Anyhow, the TEM measurement is consistent with SEM results (see Figure 2).

HRTEM Image and Elemental Mapping. TEM analysis has performed once more to acquire further information about the morphology of the CCMs samples and the crystallite of the Cu particles in them. The TEM and high resolution TEM (HRTEM) images of the representative CCMs are presented in Figure 3 as panels A and B, respectively. Figure 3A shows that the sphere is porous and the majority of Cu particles were decorated on the surface of carbon substrate. The porous characteristic of the CCMs were confirmed further by N_2 adsorption−desorption measurements (see Nitrogen Adsorption−Desorption Measurements section). The unique structure of porous sesame balls will favor the composite spheres with effective antibacterial and catalytic activity. The inset in the HRTEM image of Figure 3B gives the lattice fringes of an individual Cu nanoparticle, and a space of 0.208 nm between two lattice fringes has been calculated, which is in accordance with the (111) plane lattice parameter of fcc metallic Cu and the result is consistent with the XRD patterns as well. EDS elemental mapping analysis were carried out over the area outlined by the yellow square in Figure 3C to investigate the elemental composition and their dispersion in the CCM sample. Image D shows the dual-element map of both copper and carbon in the same CCM sample. It can be seen that the surface of the CCM was covered mainly with copper. The

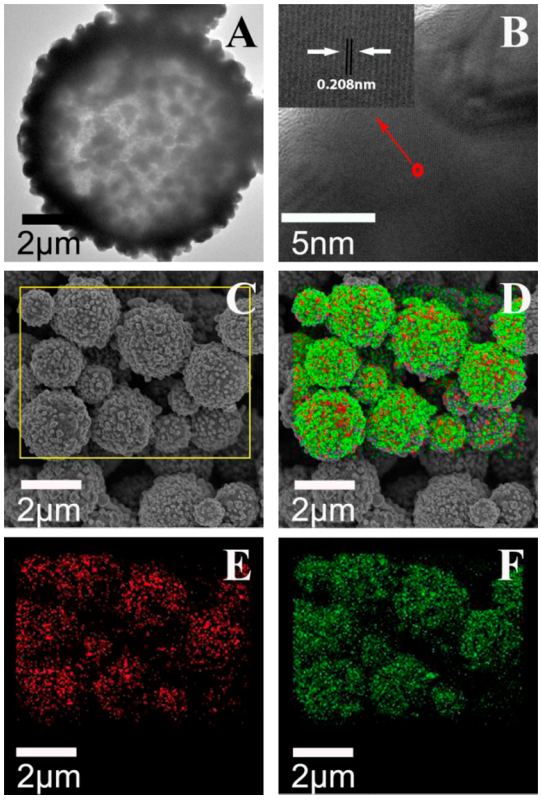

Figure 3. (A) TEM image and (B) HRTEM image of CCM-450 (5:1.5) (the inset corresponds to the magnification of the red circle area). (C) SEM image of CCM-450(5:1.5) and (D) the EDS mappings of copper/carbon (the green color represents copper element, whereas the red color corresponds to carbon element). (E) Carbon and (F) copper, respectively, corresponding to the area outlined by the yellow square in image C.

single element mapping of carbon (Figure 3E) and copper (Figure 3F), respectively, corroborates the previous observation that copper particles were dispersed onto the surface of the CCM samples uniformly, which confirm further the previous results of SEM and TEM measurements.

Thermogravimetric Analysis. To gain insight into the thermal decomposition behavior of $Cu(NH_3)_4^{2+}$/cellulose

DOI: 10.1021/acssuschemeng.5b00382
ACS Sustainable Chem. Eng. 2015, 3, 2414−2422

Table 1. BET Specific Surface Area, Pore Volume and Average Pore Width of $Cu(NH_3)_4^{2+}$/Cellulose Complex Microspheres and Those of the Corresponding CCMs

sample	BET surface area ($m^2 \cdot g^{-1}$)	pore volume ($m^3 \cdot g^{-1}$)	average pore width (nm)
5:0.5(complex)	40.6	0.10	10
5:1 (complex)	18.7	0.04	8
5:1.5 (complex)	14.5	0.03	9
5:2 (complex)	10	0.02	10
5:0.5 (calcined)	2.9	0.01	15
5:1 (calcined)	5.7	0.02	10
5:1.5 (calcined)	2.6	0.007	10
5:2 (calcined)	2.9	0.005	3

complex microspheres under nitrogen atmosphere and to find out a reasonable calcinations procedure, TGA has been carried out to two kinds of complex microspheres with different of cellulose contents (5:0.5, curve A; 5:1.5, curve B), and the results are depicted in Figure S4. One can see that there is an obvious weight loss of about 29% and 34% for $Cu(NH_3)_4^{2+}$/cellulose spheres (5:0.5) and (5:1.5), respectively, between 80 and 250 °C. The weight loss can be ascribed mainly to the decomposition of the $Cu(NH_3)_4^{2+}$ moieties in the complex spheres. A further weight loss of about 14% for both the two kinds of complex spheres between 250 and 450 °C is due to the decomposition of cellulose and residual $Cu(NH_3)_4^{2+}$. The slight differences of the thermal decomposition behavior and the total weight loss between the two kinds of $Cu(NH_3)_4^{2+}$/cellulose microspheres can be ascribed to the ratio difference between cellulose and $Cu(NH_3)_4^{2+}$ in them. For comparison and confirming the above speculation, TGA has also been performed to as-prepared $Cu(NH_3)_4(OH)_2$ solid (curve C) and pristine cellulose spheres (curve D). It can be seen from curve C that $Cu(NH_3)_4(OH)_2$ solid lost about 17% of the total weight, and then the weight kept stable from about 300 °C on, while the pristine cellulose spheres showed a drastic weight loss of about 80% between 300 and 360 °C. Moreover, it can be observed that the thermal stability of cellulose and $Cu(NH_3)_4^{2+}$ moieties in the $Cu(NH_3)_4^{2+}$/cellulose complex microspheres had been modified in comparison with that of their separated counterparts due to the association between them.

Nitrogen Adsorption−Desorption Measurements. N_2 adsorption−desorption measurements were carried out to determine the specific surface area and pore size distributions of $Cu(NH_3)_4^{2+}$/cellulose complex microspheres and the resulted CCMs. The isotherms and corresponding pore size distributions are shown in Figure S5. The isotherms of $Cu(NH_3)_4^{2+}$/cellulose complex microspheres showed very obvious hysteresis loops and capillary condensation steps (see Figure S5A), suggesting the existence of porous structure in them.[27] After the etching of $Cu(NH_3)_4^{2+}$ from the complex microspheres with acid, the specific surface area of the resulted cellulose microspheres decreases; meanwhile, the pore diameter increases. For example, for complex (5:1), the specific surface area reduces from 18.7 to 3.1 m^2/g, whereas the pore diameter increases from 8 to 24 nm (see Figure S5, panels C and D). This can be ascribed to the dissociation of the $Cu(NH_3)_4^{2+}$ species from the cellulose macromolecule chains. In comparison with the $Cu(NH_3)_4^{2+}$/cellulose complex microspheres, CCMs samples showed a narrow and irregular hysteresis loop, and the capillary condensation steps shifted to a higher relative pressure (Figure S5E), implying the reduction of porosity. The values of BET surface area, total pore volume, and average pore diameter of the samples derived from the N_2 adsorption−desorption isotherms are summarized in Table 1.

From the table, one can see that the BET surface area and total pore volume of the $Cu(NH_3)_4^{2+}$/cellulose complex microspheres decreased drastically with the increase of mass ratio of cellulose, whereas the CCMs samples showed a lower specific surface area and a smaller pore volume in comparison with their corresponding complex microspheres. Among the four different CCMs samples, CCM-450 (5:1) showed the relatively higher BET surface area and total pore volume. The reducing of specific surface area and pore volume for CCM-450 (5:05) might be due to the sintering effect of the Cu particles; whereas that for CCM-450 (5:1.5) and CCM-450 (5:2) could be attributed to the formation of the inner hollow core and macropores in the wall as have been demonstrated by SEM and TEM observations.

Antibacterial Activity. The photographs of the antibacterial test by broth dilution method for three different CCM-450 samples against *E. coli* and *S. aureus*, respectively, after a specific contact time in the same environment are presented in Figure S6. We can preliminary assess the antibacterial effect of samples according to the turbid degree of the broths. The experimental results are summarized in Table 2, and it can be deduced from

Table 2. Minimum Inhibitory Concentration (MIC) of Different CCM-450 Samples to *E. coli* and *S. aureus*

	minimum inhibitory concentration (MIC) (mg/mL)	
sample	*E. coli*	*S. aureus*
CCM-450 (5:0.5)	0.125	0.0625
CCM-450 (5:1)	0.25	0.125
CCM-450 (5:1.5)	0.5	0.25

Table 2 that (1) CCMs possess strong antibacterial effect to *S. aureus* than *E. coli*, and (2) under the condition of the same concentration of CCMs, the antibacterial efficiency improved with the increase of active ingredient of Cu in the CCMs for both the two kinds of bacteria.

Four plates containing the same content of bacteria and nutrient agar were used for the antibacterial tests by the colony forming count method, and the results are presented in Figure S7. The differences among them are that plates A and C of Figure S7 contain porous carbon microspheres only as control samples, whereas plates B and D involve CCMs. In plates B and D, there was almost no bacteria growth in the medium, indicating CCMs exhibited remarkable antibacterial activity. Whereas, the control groups (A and C) containing porous carbon microspheres were almost completely covered by bacterial colonies after contact for 24 h. The antibacterial

DOI: 10.1021/acssuschemeng.5b00382
ACS Sustainable Chem. Eng. 2015, 3, 2414−2422

efficiencies calculated based on eq S1 are listed in Table 3. The antibacterial efficiency of CCMs-450 (5:1) sample against *E. coli* and *S. aureus* were calculated to be 97% and 99.6%, respectively. This result is consistent with the MIC test. The differences of the bacterial inhibition rate of CCMs to *E. coli* and to *S. aureus* might be due to the antibacterial selectivity of metallic Cu nanoparticles. The porous structure of CCMs could promote sorption of the bacteria onto their surface, and then the active ingredient of Cu localized on the surface of carbon matrices contacted with the bacteria and damaged their functionality. The Antibacterial activities of CCM-550 samples have also been studied with the same procedure and they showed quite similar performance as these of CCM-450 samples (see Figure S8).

Table 3. Reduction in Bacterial Numbers of *E. coli* and *S. aureus* after Contact with CCMs-450 (5:1) Sample

bacterium	*E. coli*	*S. aureus*
inhibitory rate (%)	97	99.6

Catalytic Reduction of 4-Nitrophenol. The catalytic activity of these CCM samples was substantiated through 4-NP reduction to its sole product of 4-AP in the presence of $NaBH_4$ as a reductant.[28] Similar catalytic performances have been observed for both the CCM-450 series and the CCM-550 series samples (please see Figures S9–S16). We then focus on the CCM-450 samples for detailed discussion in the following section. The extent of reaction can be followed by measuring the change in UV–vis absorbance at 400 and 300 nm.[29] As can be seen in Figure 4A, the pure 4-NP solution showed a characteristic absorption peak at 317 nm, and the absorption peak shifted to 400 nm after the addition of freshly prepared $NaBH_4$ aqueous solution, which corresponds to a color change from light yellow to bright yellow due to the formation of 4-nitro-phenolate ion in alkaline condition. The bright yellow solution was very stable, and the absorption was unchanged even after adding superfluous $NaBH_4$ solution for more than 2 h, which confirmed that the reduction did not proceed in the presence of only $NaBH_4$ solution. In contrast, the catalytic activity of CCMs toward 4-NP reduction is convincingly demonstrated by the UV–vis absorption spectra in Figure 4B. With the introduction of 5.0 mg of CCM-450(x:y) (x:y = 5:0.5, 5:1, 5:1.5, and 5:2, respectively) into the reaction solution, the absorption peak at 400 nm immediately disappeared and a new peak at 300 nm increased at once. The new absorption at 300 nm is the characteristic peak of 4-AP and it appearance reveals the reduction of 4-NP to 4-AP.[30] Because of the strong adsorbing ability of the porous CCMs catalyst, $NaBH_4$ and 4-NP could be rapidly adsorbed on the surface of CCMs, where the Cu particles could relay electrons from the donor of BH_4^- to the acceptor of 4-NP, and promote the occurrence of reduction reaction. After the electrons were transferred to the Cu nanoparticles, the hydrogen atoms derived from $NaBH_4$ attacked 4-NP molecules to reduce it.[31] As has been demonstrated by Figure 4C, when CCMs were added to the reaction system, the bright yellow solution changed immediately to colorless. These results confirmed that the CCMs were effective catalysts for the reduction of 4-NP to 4-AP. After the catalytic process, pure 4-AP can be isolated from the solution by combining extraction with recrystallization, and isolated yield of 4-AP more than 95% has been obtained. For comparison, a control test was conducted with a mixture of 4-NP, $NaBH_4$, and porous carbon microspheres without Cu particles. Obviously, there was little decrease in the absorbance at 400 nm as monitored by UV–vis spectrometer due to the physical adsorption of the nitro compound on CCMs, whereas no absorption peak assigned to 4-AP appeared at around 300 nm, indicating that the catalytic reduction of 4-NP could not occur at all without Cu ingredients and confirming the role of metallic Cu nanoparticles as a catalyst in the reduction process (Figure 4D).

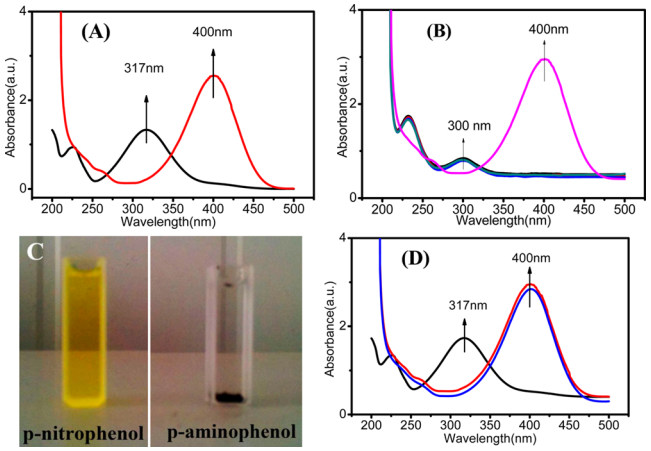

Figure 4. UV–vis spectra of (A) 4-NP in the absence (the black curve) and presence (the red curve) of $NaBH_4$ solution. (B) UV–vis spectra for the catalytic reduction of 4-NP using CCM-450 (x:y) as catalyst. (C) Photographs of the reduction of 4-NP by $NaBH_4$ in the presence of CCM catalyst. (D) UV–vis spectra for the catalytic reduction of 4-NP using porous carbon microspheres as catalyst.

The kinetics of catalytic reduction of 4-NP to 4-AP over the CCMs with different Cu contents were investigated, and the typical time-dependent absorption spectra of the reaction solution are shown as panels A–D of Figure S9. It can be observed from the figures that the reaction time of the catalytic reduction of 4-NP to 4-AP turned to shorter with the increase of Cu content in the CCMs. As the initial concentration of $NaBH_4$ is largely excess in comparison to 4-NP, the the pseudo-first-order kinetics can be applied for the evaluation of rate constants in this reaction.[32] Therefore, the rate equation can be written as

$$\frac{dc_t}{dt} = -kc_t \tag{1}$$

where c_t is the concentration of 4-NP at time t and k is the rate constant. Integrating with boundary conditions of when $t = 0$, $c_t = c_0$ and when $t = t$, $c_t = c_t$ yields

$$\ln\left(\frac{c_t}{c_0}\right) = -kt \tag{2}$$

Considering that the ratio of absorbance A_t of 4-NP at time t to its value A_0 measured at $t = 0$ must be equal to the concentration ratio c_t/c_0 of 4-NP, thus the above equation can be rewritten as

$$\ln\left(\frac{A_t}{A_0}\right) = -kt \tag{3}$$

The corresponding linear correlations between $\ln(A_t/A_0)$ versus time t are shown in Figure S9E. The apparent rate

DOI: 10.1021/acssuschemeng.5b00382
ACS Sustainable Chem. Eng. 2015, 3, 2414–2422

constants (kapp) were calculated, and the results are listed in Figure S9F. It is observed from the figure that the order of the catalytic activity for the different CCMs was A < B < C < D. The content of Cu in the composite spheres affects significantly the catalytic activities of CCMs, confirming the role of Cu in the catalytic reduction.

To ascertain the influence of catalyst quantity on the kinetics of the catalytic reduction, experiments were carried out over CCM-450 (5:2) with four different dosages (see Figure S10: A, 0.5 g/L; B, 1g/L; C, 1.5 g/L; D, 2 g/L). The time-dependent absorption spectra and plots of $\ln(A_t/A_0)$ against reaction time of the reaction solution for catalytic reduction of 4-NP over different amounts of catalyst are presented in Figure S10E, and it showed that with the increase of catalyst quantity, the rate constant increases as well. The result is reasonable because the increase in catalyst amount provided more catalytic sites for the reaction. The dependences of rate constants on $NaBH_4$ and 4-NP concentrations are also studied and the results are presented as Figures S11 and S12, respectively. It is observed from the figures that the rate constant of catalytic reduction significantly increases with the increase of $NaBH_4$ concentration, whereas, it decreases with the increase of the 4-NP concentration. The mechanism of the catalytic reaction could be explained by the Langmuir−Hinshelwood mechanism. $NaBH_4$ ionized in water to offer BH_4^-, providing surface hydrogen for the reaction. The surface hydrogen first transferred to copper particles, and then reacted with 4-NP to yield 4-AP.[33] BH_4^- acted as the electron donor, whereas 4-NP acted as the electron acceptor.[34] The CCMs served as catalyst to provide active sites for promoting the reaction. These results demonstrated that all these variable parameters are very essential to the reduction of 4-NP, and in a practical application one can optimize the catalytic effect by adjusting the quantity of the catalyst and the concentration of the reactants for a selected CCM catalyst.

Recyclability and Stability. The structure stability of the composite spheres and the composition stability of metal particles are crucial to their applications for all the supported catalysts. Usually, catalysts based on metals suffer from oxidizing of oxygen during storage and from poisoning by the reaction intermediate during the catalytic process.[35] Thus, exploring a catalyst with excellent reusability and high stability is necessary. It has been demonstrated that the CCMs could keep their integrated structure even under the irradiation of ultrasonication for more than 1 h, indicting high structure stability. The recyclability of catalyst upon the reduction was carried out for five successive cycles, and the result is presented in Figure S17. Only a very slight decrease of conversion efficiency was observed, suggesting their high catalytic stability. In our experiments, after each run of the catalytic reaction, the catalyst microspheres were separated easily by centrifugation, while the supernatant was removed by decantation and then fresh reactant solution was introduced for the consequent reactions. The excellent stability of the catalytic activity could be attributed to the low loss of copper content during the reduction cycles and to the structural stability of the solids.[36]

The composition of the CCM samples stored in ambient air for 6 months and those upon catalytic reaction have been studied by recording their powder XRD patterns (see Figure S18) and the XPS surveys (see Figure S19). All these stored samples showed quite similar XRD patterns with those of the as-prepared ones, whereas the recovered CCM-450 catalysts showed the presence of peaks corresponding to fcc Cu together with a considerably weak peak which is related to Cu_2O (see Figure S18b). XPS full surveys of the as-prepared CCM-450 (5:2), the one stored at ambient air for 6 months, and the sample used as catalyst after 5 cycles showed the presence of carbon (285 eV), oxygen (532 eV), and copper (933 eV) (see Figure S19a).[37] High-resolution scans at the Cu 2p region showed binding energy peaks corresponding to Cu $2p_{3/2}$ and Cu $2p_{1/2}$ photoelectron transitions, respectively. For the as-prepared CCM-450 (5:2), the Cu $2p_{3/2}$ and Cu $2p_{1/2}$ appear at 932.6 and 952.5 eV, which can be characteristic of Cu in the Cu^+ or Cu^0 oxidation state.[38] The stored and the recovered CCM-450 (5:2) samples, on the other hand, showed shoulders beside the main peaks and accompanied by shakeup satellite peaks. They can be deconvoluted into two peaks each for Cu $2p_{3/2}$ at 932.8 and 934.3 eV and Cu $2p_{1/2}$ at 952.6 and 955.2 eV (see Figure S19b). The peaks for Cu $2p_{3/2}$ at 934.3 eV, Cu $2p_{1/2}$ at 955.2 eV, and the shakeup satellite peaks around 943 and 963 eV are characteristic of Cu in the Cu^{2+} oxidation state from CuO formed during storage and recycling. It is difficult to distinguish Cu^0 from Cu^+ by only the Cu 2p XPS peaks; however, one can identify them by the position of their LMM-2 auger transitions in the spectra, which appear at 568 and 570 eV for Cu and Cu_2O, respectively.[39] There is a peak at about 570 eV in the XPS spectra for the three samples. Furthermore, isolated Auger electron spectra of Cu LMM were recorded at a kinetic energy of 916.8 eV, which can be converted into a binding energy of about 569.8 eV (see Figure S19c). On the basis of these facts, one then can conclude that the Cu $2p_{3/2}$ peak at 932.6 eV is related to Cu_2O, which means that the Cu particles in the as-prepared CCMs are covered with a thin Cu_2O layer. XPS is a surface-sensitive analytical technique useful for the identification of elements present on the surfaces, whereas the XRD technique can detect composition of the bulk. The XPS results are, nevertheless, consistent with the XRD measurement. It is the case that Cu nanoparticles are sensitive to oxygen; therefore, it is reasonable that the Cu particles were covered with a thin cuprum oxide. However, it is interesting to note that partial oxidation of the Cu particle surface does not influence the catalytic efficiency obviously, and the catalyst is reused for five cycles with high activity. The morphology of the recovered CCMs was investigated by SEM and was found to be comparable with that of the as-prepared CCMs (see Figure S20).

CONCLUSIONS

A sustainable and versatile process for *in situ* formation of metallic Cu particles decorated porous carbon microspheres (CCMs) has been established. The spray drying has been proved to be an efficient technique for the preparation of porous microspheres of $Cu(NH_3)_4^{2+}$/cellulose complex using the cuprammonia cellulose aqueous solution as raw materials. CCMs possessing a unique sesame ball structure can be deduced *in situ* by calcining the $Cu(NH_3)_4^{2+}$/cellulose complex microspheres at 450 or 550 °C. The size of the Cu particles in the CCMs can be affected by the calciantion temperature. The coordination between the $Cu(NH_3)_4^{2+}$ species and the hydroxyl groups of the cellulose macromolecules plays important role in directing the dispersion of the Cu particle in the final composite CCMs. The resultant CCMs displayed great potential as a high efficiency antimicrobial agent to both Gram-positive *Staphylococcus aureus* and Gram-negative *Escherichia coli*, and also as a high performance catalyst for the conversion of 4-nitrophenol to 4-aminophenol using $NaBH_4$

DOI: 10.1021/acssuschemeng.5b00382
ACS Sustainable Chem. Eng. 2015, 3, 2414−2422

aqueous solution as a reductant in a mild condition. The present work demonstrated also that some conventional materials such as the ancient cuprammonia cellulose aqueous solution and traditional techniques, for example, spray drying, can rebloom in modern science and technology for advanced applications, and more importantly will trigger the attention of researchers to these traditional materials or techniques. For instance, one can extend the reported preparation method and the coordination effect strategy to other kinds of metal or metal oxide decorated carbon composite spheres using different transition metal complex solutions of cellulose as precursors, such as Fe(II), Co (II), Zn(II), Ni(II), and explore their potential applications in catalysis and energy storage. Such work is still underway in our group.

■ ASSOCIATED CONTENT

Supporting Information

The Supporting Information is available free of charge on the ACS Publications website at DOI: 10.1021/acssuschemeng.5b00382.

A more detailed description of the test procedures of the antibacterial properties, XRD patterns of the CCM-550 series samples, SEM images of the $Cu(NH_3)_4^{2+}$/cellulose microspheres, TEM images of the two series of CCMs, TGA curves of the $Cu(NH_3)_4^{2+}$/cellulose spheres (5:0.5 and 5:1.5), nitrogen adsorption−desorption isotherms and the corresponding pore size distribution of the $Cu(NH_3)_4^{2+}$/cellulose complex spheres and that of CCMs, photographs of the antibacterial test results against *E. coli* and *S. aureus*, time-dependent absorption spectra of the catalytic reaction solution, curve of conversion efficiency against number of cycles, XRD patterns of CCM-450 (*x*:*y*) after storing for 6 months, and SEM images of the recovered CCM-450(*x*:*y*) catalysts after 5 catalytic cycles (PDF).

■ AUTHOR INFORMATION

Corresponding Author

*H. Li. E-mail: lhl@qdu.edu.cn.

Notes

The authors declare no competing financial interest.

■ ACKNOWLEDGMENTS

This work is supported by the National Key Project on Basic Research (Grant No. 2012CB722705), the National High Technology Research and Development Program of China (Nos. 2013BAG26B02 and 2014AA052303), and the Natural Science Foundation of China (Nos. 21103096 and U1232104). Y. Wang thanks the financial support from the Top-notch Innovative Talent Program of Qingdao City (Grant no. 13-CX-8) and the Taishan Scholar Program of Shandong Province.

■ REFERENCES

(1) Gholinejad, M.; Jeddi, N. Copper Nanoparticles Supported on Agarose as a Bioorganic and Degradable Polymer for Multicomponent Click Synthesis of 1,2,3-Triazoles under Low Copper Loading in Water. *ACS Sustainable Chem. Eng.* **2014**, *2*, 2658−2665.

(2) Manthiram, K.; Beberwyck, B. J.; Alivisatos, A. P. Enhanced electrochemical methanation of carbon dioxide with a dispersible nanoscale copper catalyst. *J. Am. Chem. Soc.* **2014**, *136*, 13319−13325.

(3) Cioffi, N.; Torsi, L.; Ditaranto, N.; Tantillo, G.; Ghibelli, L.; Sabbatini, L.; Bleve-Zacheo, T.; D'Alessio, M. D.; Zambonin, P. G.; Traversa, E. Copper Nanoparticle/Polymer Composites with Antifungal and Bacteriostatic Properties. *Chem. Mater.* **2005**, *17*, 5255−5262.

(4) Xiong, X.; Cai, L.; Jiang, Y.; Han, Q. Eco-efficient, Green, and scalable synthesis of 1, 2, 3-triazoles catalyzed by Cu(I) catalyst on waste oyster shell powders. *ACS Sustainable Chem. Eng.* **2014**, *2*, 765−771.

(5) Chakrapani, V.; Behlol, K.; Ahmed, V.; Kumar, V.; Ganapathy, V.; Anthony, S. P.; Anbazhagan, V. A facile route to synthesize casein capped copper nanoparticles: an effective antibacterial agent and selective colorimetric sensor for mercury and tryptophan. *RSC Adv.* **2014**, *4*, 33215−33221.

(6) Ranu, B. C.; Dey, R.; Chatterjee, T.; Ahammed, S. Copper nanoparticle-catalyzed carbon-carbon and carbon-heteroatom bond formation with a greener perspective. *ChemSusChem* **2012**, *5*, 22−44.

(7) Gewirth, A. A.; Thorum, M. S. Electro reduction of dioxygen for fuel-cell applications: materials and challenges. *Inorg. Chem.* **2010**, *49*, 3557−3566.

(8) Park, B. K.; Jeong, S.; Kim, D.; Moon, J.; Lim, S.; Kim, J. S. Synthesis and size control of monodisperse copper nanoparticles by polyol method. *J. Colloid Interface Sci.* **2007**, *311*, 417−424.

(9) Benavente, E.; Lozano, H.; González, G. Fabrication of copper nanoparticles: advances in synthesis, morphology control, and chemical stability. *Recent Pat. Nanotechnol.* **2013**, *7*, 108−132.

(10) Kanninen, P.; Johans, C.; Merta, J.; Kontturi, K. Influence of ligand structure on the stability and oxidation of copper nanoparticles. *J. Colloid Interface Sci.* **2008**, *318*, 88−95.

(11) Khdary, N. H.; Ghanem, M. A.; Merajuddine, M. G.; Bin Manie, F. M. Incorporation of Cu, Fe, Ag, and Au nanoparticles in mercapto-silica (MOS) and their CO_2 adsorption capacities. *J. CO2 Util.* **2014**, *5*, 17−23.

(12) Kaur, P.; Hupp, J. T.; Nguyen, S. T. Porous Organic Polymers in Catalysis: Opportunities and Challenges. *ACS Catal.* **2011**, *1* (7), 819−835.

(13) Yang, Y.; Chiang, K.; Burke, N. Porous carbon-supported catalysts for energy and environmental applications: A short review. *Catal. Today* **2011**, *178*, 197−205.

(14) Zhang, S.; Chen, L.; Zhou, S.; Zhao, D.; Wu, L. Facile Synthesis of hierarchically ordered porous carbon via in situ self-assembly of colloidal polymer and silica spheres and its use as a catalyst support. *Chem. Mater.* **2010**, *22*, 3433−3440.

(15) Ferrando, R.; Jellinek, J.; Johnston, R. L. Nanoalloys: From Theory to Applications of Alloy Clusters and Nanoparticles. *Chem. Rev.* **2008**, *108*, 845−910.

(16) Lou, X. W.; Yuan, C.; Rhoades, E.; Zhang, Q.; Archer, L. A. Encapsulation and Ostwald Ripening of Au and Au-Cl Complex Nanostructures in Silica Shells. *Adv. Funct. Mater.* **2006**, *16*, 1679−1684.

(17) Dupont, J.; Fonseca, G. S.; Umpierre, A. P.; Fichtner, P. F.; Teixeira, S. R. Transition-metal nanoparticles in imidazolium ionic liquids: recyclable catalysts for biphasic hydrogenation reactions. *J. Am. Chem. Soc.* **2002**, *124*, 4228−4229.

(18) Titirici, M. M.; White, R. J.; Brun, N.; Budarin, V. L.; Su, D. S.; del Monte, F. Sustainable carbon materials. *Chem. Soc. Rev.* **2015**, *44*, 250−290.

(19) Klemm, D.; Heublein, B.; Fink, H. P.; Bohn, A. Cellulose: fascinating biopolymer and sustainable raw material. *Angew. Chem., Int. Ed.* **2005**, *44*, 3358−3393.

(20) Wang, Q.; Fu, A.; Li, H.; Liu, J.; Guo, P.; Zhao, X. S.; Xia, L. H. Preparation of cellulose based microspheres by combining spray coagulating with spray drying. *Carbohydr. Polym.* **2014**, *111*, 393−399.

(21) Kauffmann, G. B. A brief History of Cuprammonium Rayon. In *Manmade Fibers: Their Origin and Development*; Seymour, R. B., Porter, R. S., Eds.; Kluwer Academic Publishers: New York, 1993.

(22) Shahverdi, A. R.; Fakhimi, A.; Shahverdi, H. R.; Minaian, S. Synthesis and effect of silver nanoparticleson the antibacterial activity of different antibiotics against staphylococcus aureus and escherichia coli. *Nanomedicine* **2007**, *3*, 168−171.

(23) Yu, Q.; Fu, A.; Li, H.; Liu, H.; Lv, R.; Liu, J.; Guo, P.; Zhao, X. S. Synthesis and characterization of magnetically separable Ag nano-

particles decorated mesoporousFe_3O_4@carbon with antibacterial and catalytic properties. *Colloids Surf., A* **2014**, *457*, 288−296.
(24) Bruna, J. E.; Galotto, M. J.; Guarda, A.; Rodriguez, F. A novel polymer based on $MtCu^{2+}$/cellulose acetate with antimicrobial activity. *Carbohydr. Polym.* **2014**, *102*, 317−323.
(25) Wang, M.; Tian, D.; Tian, P.; Yuan, L. Synthesis of micron-SiO_2@nano-Ag particles and their catalytic performance in 4-nitrophenol reduction. *Appl. Surf. Sci.* **2013**, *283*, 389−395.
(26) Kassaee, M. Z.; Buazar, F.; Motamedi, E. Effects of current on arc fabrication of Cu nanoparticles. *J. Nanomater.* **2010**, *2010*, 403197.
(27) Li, H. L.; Sang, J.; Zhao, J.; Fu, A.; Liu, H.; Xu, M.; Pang, G.; Zhao, X. S. Preparation of magnetically separable mesoporous Co@carbon/silica composites by the RAPET method. *New J. Chem.* **2012**, *36*, 2308−2315.
(28) Pradhan, N.; Pal, A.; Pal, T. Silver nanoparticle catalyzed reduction of aromatic nitro compounds. *Colloids Surf., A* **2002**, *196*, 247−257.
(29) Zhu, Y.; Shen, J.; Zhou, K.; Chen, C.; Yang, X.; Li, C. Multifunctional magnetic composite microspheres with in situ growth Au nanoparticles: a highly efficient catalyst system. *J. Phys. Chem. C* **2011**, *115*, 1614−1619.
(30) Pradhan, N.; Pal, A.; Pal, T. Catalytic reduction of aromatic nitrocompounds by coinage metal nanoparticles. *Langmuir* **2001**, *17*, 1800−1802.
(31) Le, X.; Dong, Z.; Zhang, W.; Li, X.; Ma, J. Fibrous nano-silica containing immobilized Ni@ Au core−shell nanoparticles: a highly active and reusable catalyst for the reduction of 4-nitrophenol and 2-nitroaniline. *J. Mol. Catal. A: Chem.* **2014**, *395*, 58−65.
(32) Praharaj, S.; Nath, S.; Ghosh, S. K.; Kundu, S.; Pal, T. Immobilization and recovery of Au nanoparticles from anion exchange resin: resin-bound nanoparticle matrix as a catalyst for the reduction of 4-nitrophenol. *Langmuir* **2004**, *20*, 9889−9892.
(33) Bhui, D. K.; Misra, A. Synthesis of worm like silver nanoparticles in methyl cellulose polymeric matrix and its catalytic activity. *Carbohydr. Polym.* **2012**, *89*, 830−835.
(34) Pootawang, P.; Lee, S. Y. Rapid synthesis of Ag nanoparticles-embedded mesoporous silica via solution plasma and its catalysis for 4-nitrophenol reduction. *Mater. Lett.* **2012**, *80*, 1−4.
(35) Lin, F.; Doong, R. Bifunctional Au-Fe_3O_4 heterostructures for magnetically recyclable catalysis of nitrophenol reduction. *J. Phys. Chem. C* **2011**, *115*, 6591−6598.
(36) Sun, Y.; Xu, L.; Yin, Z.; Song, X. Synthesis of copper submicro/nanoplates with high stability and their recyclable superior catalytic activity towards 4-nitrophenol reduction. *J. Mater. Chem. A* **2013**, *1*, 12361−12370.
(37) Moulder, J. F.; Stickle, W. F.; Sobol, P. E.; Bomben, K. D. In *Handbook of X-ray photoelectron spectroscopy*; Chastain, J., King, R. C., Jr., Eds.; Physical Electronics Division, Perkin-Elmer: Eden Prairie, MN, 1995; pp 40, 44, and 86.
(38) Ghijsen, J.; Tjeng, L. H.; van Elp, J.; Eskes, H.; Westerink, J.; Sawatzky, G. A.; Czyzyk, M. T. Electronic structure of Cu_2O and CuO. *Phys. Rev. B: Condens. Matter Mater. Phys.* **1988**, *38*, 11322−11330.
(39) Ghodselahi, T.; Vesaghi, M. A.; Shafiekhani, A.; Baghizadeh, A.; Lameii, M. XPS study of the Cu@Cu_2O core-shell nanoparticles. *Appl. Surf. Sci.* **2008**, *255*, 2730−2734.

DOI: 10.1021/acssuschemeng.5b00382
ACS Sustainable Chem. Eng. 2015, 3, 2414−2422